Marine carbon sink dominated by biological pump after temperature overshoot

Supplementary Material

Contents:

Supplementary Methods
Supplementary Results
Supplementary Tables (S1 to S3)
Supplementary Figures (S1 to S8)
Supplementary Reference

Supplementary Methods:

Sensitivity experiments

In order to demonstrate the robustness of our main findings, we carried out idealized sensitivity experiments with different model setups (circulation strength and biogeochemistry), modified assumptions about negative emissions during ramp-down and different peak pCO_2^{atm}. In experiment 2xCO2_slowcirc, (2xCO2_fastcirc) maximum overturning was 15.5 Sv (19.0 Sv) at the beginning of the experiment, i.e. a little smaller (larger) compared with the default model setup (17.2 Sv). This was achieved by changing the model vertical background diffusivity (Kv) to values slightly lower (larger) than in the default experiment (see [1] for rational and Tab. S1 for values). We also performed experiments with the default circulation, but with slightly modified organic matter sinking parameterization. While in the default model sinking speed increased with (6m/d) / 100m, experiment 2xCO2_fastsink assumed (8m/d) / 100m and experiments 2xCO2_slowsink (4m/d) / 100m. Prior to sensitivity experiments, the respective model variants had undergone a full model spinup, like the default model, which had been carried out with prescribed preindustrial pCO_2^{atm} and climate conditions. Differences in overturning and sinking parameterization hence caused also differences in the initial DIC^{remin} stocks of the models (compare Tab. S1).

Further sensitivity experiments performed with the default model setup explored potential effects concerning the prescribed pCO_2^{atm} decrease rate after peak-pCO_2. In addition to the default model (REVERSE), which applied a decrease rate of -1%/year, we carried out model experiments with decrease rates ranging between -0.9%/year and -0.1%/year. The experiment with a decrease rate of -0.2%/year showed a deep convection event during the

experiment period. Similar events have been reported from climate change transient experiments [2,3] but are beyond the scope of this research. Another sensitivity experiment repeated REVERSE, however, with a ramp-up period of 140 years with +1%/year until reaching $4xCO_2$ and a subsequent ramp-down period of another 140 years with -1%/year change until reaching preindustrial pCO_2 again.

We also performed an experiment with moderate temperature overshoot. This experiment branched off from REVERSE after peak pCO_2 and peak ΔSAT had been passed and when ΔSAT was again close to the climate target of $\Delta SAT=1.5°C$ and continue with net-zero CO_2-emissions thereafter. Given the temporal resolution of the restart files written during REVERSE, we branch off one experiment at $\Delta SAT=1.56°C$. An additional experiment branches of when a similar ΔSAT (1.51°C) was reached during the ramp-up phase. While the former experiment had a history of pCO_2 and temperature overshoot, the latter had not.

All sensitivity experiments were run for 500 years in total.

Experiments to compute climate feedback parameters

In addition to the coupled 4xCO2 experiment described above we also carried out a biogeochemically-only coupled experiment (4xCO2_BGC). In this experiment atmospheric pCO_2 increased as in 4xCO2, but this increase did not affect the climate [4], which was held stable at preindustrial conditions. Since our biogeochemical model did not include biological CO_2-concentration feedbacks and since the land model, which may feature potential albedo (climate) feedbacks to increasing atmospheric pCO_2, was excluded, the marine CO_2-uptake from BGC simulated the uptake of anthropogenic CO_2 in the absence of climate change. In a BGC experiment, as carried out with our model, DIC^{remin} does not change with time, except for the model's regular seasonal cycle. Following [5], we used the combination of 4xCO2 and 4xCO2_BGC during the 1%/year pCO_2 increase phase in order to estimate standardized marine carbon-climate and carbon-concentration feedback parameters.

Supplementary Results

Model parameter uncertainty

First, we explored with additional simulations the sensitivity of marine carbon storage to the initial state of the ocean model. We did so by changing model parameters that either affect circulation (ocean physics) or the particle flux parameterization (ocean biogeochemistry) *(see SI Methods for details)*. Starting from their own model spinup, experiments followed the experimental protocol and atmospheric pCO_2 boundary conditions of REVERSE (see Online Methods for details). All experiments showed the multi-centennial dominance of ΔDIC^{remin} compared with ΔDIC^{pre} (Fig. S3), though with slightly different timing when the remineralized pool starts to dominate over the preformed carbon pool ($\Delta DIC^{remin} > \Delta DIC^{pre}$). We found a first order negative relationship between maximum overturning and intersection point (Fig. S3c, d; Tab. S2), i.e. a slower circulation delayed the point where ΔDIC^{remin} equals ΔDIC^{pre}. Similarly, a deeper penetration of organic matter in the ocean (experiment 2xCO2_fastsink) showed a delayed intersection point compared with REVERSE and the experiment 2xCO2_slowsink (Fig S3a, b; Tab S2).

Speed of pCO_2^{atm} decrease during ramp-down

Second, we tested the effect of varying the intensity of net-negative emissions. This was done by varying the prescribed rate of decrease of atmospheric pCO_2 during the ramp-down phase between -1% (REVERSE) and -0.1% in 0.1% steps (Fig. S4a). All but the last two experiments (-0.2%, -0.1%) showed periods with ΔDIC^{remin} being larger than ΔDIC^{pre} (Fig. S4c, d). With slower pCO_2^{atm} recovery (lower net-negative emissions, Fig S4b), however, the occurrence of dominant ΔDIC^{remin} (solid lines in Fig. S4c) became delayed until it disappeared in the last two experiments.

Experiment with 4xCO2 peak pCO_2^{atm}

Finally, we tested the effect of higher peak CO_2 concentrations: in experiment 4xCO2, in which pCO_2^{atm} peaked at four times the preindustrial CO_2, marine CO_2 uptake was much larger compared with REVERSE, but again the ocean lost rapidly carbon from the DIC^{pre} pool when the atmospheric pCO_2 decreased after peak concentrations. Like in REVERSE, DIC^{remin} increased (in absolute and relative contribution) until the end of the ramp- down period and

thereafter it decreased only very slowly (Fig. S5). However, given a longer ramp-up and ramp-down period the intersection-point ($\Delta DIC^{remin} = \Delta DIC^{pre}$) was reached only in year 410.

<u>Earth System feedback analysis</u>

The CO_2-uptake dynamics of our model compared well with that of other climate models, that include carbon-climate feedback of similar strength, and with observations, supporting the plausibility of our projections of an increasing role of DIC^{remin} on centennial time scales and particularly under net-negative emissions. We computed carbon-climate and carbon-concentrations ocean feedback parameters (γ_O and β_O, respectively) using a standardized approach used in climate research (e.g. [5]). In this approach a combination of ramp-up phase results of the fully coupled model experiment with 1%/year CO_2 increase run until reaching four times the preindustrial atmospheric pCO_2 (here experiment 4xCO2_REVERSE) and the respective biogeochemically-only coupled counterpart version (4xCO2_BGC) are compared. Our value of the marine carbon-concentration feedback parameter, β_O, derived from this analysis was 0.85 Pg C / ppm, which is within the range reported for CMIP5 and CMIP6 models (0.82±0.07 Pg C / ppm, 0.79±0.07 Pg C / ppm, respectively; mean ± standard deviation; [5]). Our value of the marine carbon-climate feedback parameter, γ_O, was -22.3 Pg C / °C, which is at the high-end sensitivity reported for CMIP5 and CMIP6 models (-17.3±3.8 Pg C / °C and -17.2±5 Pg / °C, respectively [5]. Sensitivity experiments with slightly stronger (weaker) overturning (2xCO2_fastcirc and 2xCO2_slowcirc, respectively) showed carbon-climate sensitivities which were stronger (weaker) by about 10% and carbon concentration feedback parameters which were larger (smaller) by about 5%, and vice versa. Further, the default model variant used here, when confronted with historical CO_2-emissions forcing [6], was able to well reproduce global and basin scale marine CO_2 uptake observed over recent decades and also compared well with the range of CMIP-model CO_2 uptake (Tab. S3).

<u>Understanding respiration and oxygen dynamics benefits two research fields: the contribution of the biological carbon pump (BCP) to marine carbon storage and deoxygenation</u>

Contemporary changes of biological pump carbon (ΔDIC^{remin}) cannot be measured directly, but may be estimated based on monitoring marine oxygen. Simultaneous measurements of

oxygen, temperature and salinity allow for the quantification of oxygen saturation and the accumulated oxygen deficit. This deficit, the apparent oxygen utilization (AOU), can be converted to carbon units by applying a global average O_2:C ratio and provides a first order observational constraint of ΔDIC^{remin} [7]. This first order estimate of ΔDIC^{remin} is likely a conservative (low) estimate of ΔDIC^{remin}, for example since it assumes that the accuracy of the O_2^{sat} assumption (AOU = $O_2^{sat} - O_2$, with O_2^{sat} = f(T, S), oxygen saturation computed from temperature and salinity) is perfect and in particular does not change with time. This assumption assumes that the oxygen disequilibrium can be neglected or, at least, does not change with climate change, which is unlikely since global warming causes shrinking sea ice cover, and hence the oxygen disequilibrium to decrease ([6], see their SI Figs. S5, S6). We compared ΔDIC^{remin} from the explicit DIC^{remin} tracer in REVERSE with ΔDIC^{remin} computed from a true oxygen utilization tracer (TOU tracer, [8]) and from AOU computed from model output (Fig. S6a). While DIC^{remin} and TOU tracer based estimates almost perfectly agreed (solid and long dashed lines), the AOU based estimate (short dashed line) underestimated ΔDIC^{remin} by 23.1 (±2.7)% in REVERSE. This underestimate was explained by considerable differences in transient changes of computed saturated oxygen and the preformed oxygen tracer of the model, respectively (Fig. S6b), i.e. changes in the oxygen disequilibrium. In the real ocean, such a change of the oxygen disequilibrium is to be expected, but hard to quantify.

The real ocean has been found to lose oxygen in the course of global warming [9]. While in the upper ocean (0-1200m) most of this loss was due to the effect of warming on oxygen solubility and hence unrelated to biological pump carbon, deep ocean (> 1200 m) deoxygenation was mostly due to an increase in AOU (Ref [10]) and hence indicative of an increase in DIC^{remin}.

In this context it is worrisome that many climate models, including our model, have been found to underestimate deoxygenation in the recent-50yr hindcast by about a factor two on average [11], compared with observations, which for the time period 1960 to 2010, suggest an oxygen loss of 96 Tmol /yr (Ref [10]), translating into an underestimate of a corresponding increase of ocean DIC^{remin}. The cause of this underestimate is not well understood [12,13].

Forced with historical CO_2-emissions [6], our default model variant showed a similar underestimate (38% of the observed rate, 37 Tmol/yr). In our model, about 22% of this globally integrated oxygen loss was thermally driven (i.e. by surface ocean warming affecting O_2-solubility), the rest (28.8 Tmol/yr) was explained by an increase in apparent oxygen utilization (AOU), likely associated to increasing stratification and circulation slow down [6]. Observations have suggested a similar relative partitioning between warming-solubility driven (e.g. 15% in [10]) and AOU driven deoxygenation. This suggests that the majority of our model's underestimate of deoxygenation is likely to be explained by an underestimate of the increase in AOU.

Further, observed trends of global ocean deoxygenation may be uncertain given the scarcity of oxygen data in the deep ocean over recent decades. Acknowledging this uncertainty, we suggest that the underestimate of simulated AOU-change during the historical period may further point to a potential underestimate of DIC^{remin} change in the past. We speculate that this may also apply for projection into the future and our idealized model experiments. This may indicate that our estimate of the role of DIC^{remin} for the longer-term marine storage of CO_2 in overshoot scenarios, like those studied in this work, was a conservatively low estimate. Ongoing global efforts to use oxygen sensors on ARGO floats [14], however, offer the unique opportunity to monitor future global integrated changes of DIC^{remin} as well as its geographical distribution. These data can contribute in the future to constrain the representation of oxygen dynamics in ocean models, and thereby may become an important component to correctly project the long-term future storage of excess DIC in the ocean.

The Southern Ocean is a major return path of old waters from the deep ocean enriched with the products of organic matter degradation (oxygen deficit and DIC^{remin}) and from $CaCO_3$ dissolution, the latter enriching waters with DIC and alkalinity (in a 1:2 ratio). This causes complex vertical and horizontal patterns of the resulting potential partial pressure of CO_2 (ref [15]) relative to the time varying atmospheric pCO_2. Since the Southern Ocean also is the critical region from which elevated DIC^{remin} developed under net-negative CO_2 emissions (see Fig. 2 e, h), we suggest further research to better understand the processes that control the Southern Ocean accumulation of DIC^{remin}, but also of the degradation products of $CaCO_3$-dissolution, on centennial time scales and under anthropogenic climate change.

Supplementary Tables

Tab. S1: Experiment and model characteristics in year 0 of the respective experiments (i.e. end of spinup). For details on the experiments, see the Supplementary Methods section.

Experiment	Maximum overturning in Sv	Sinking speed increase with depth in (m/d)/100m	DIC inventory in Pg C	DIC^{remin} in Pg C
REVERSE, MODERATE, 2xCO2_ii, 4xCO2, 4xCO2_BGC	17.2	6	37505	1285
2xCO2_slowcirc	15.5	6	37599	1308
2xCO2_fastcirc	19.0	6	37399	1246
2xCO2_slowsink	17.2	4	37234	1106
2xCO2_fastsink	17.2	8	37698	1383

2xCO2_ii refers to experiment 2xCO2_0.9 to 2xCO2_0.1, see Tab. S2

Tab. S2: Overview of experimental characteristics during the transient period. Cumulative emissions is the cumulative of compatible emissions under the prescribed atmospheric pCO_2-scenario with respect to an ocean-atmosphere system. Compatible emissions quantify the deviation from initial model Earth System carbon at preindustrial time that emerges in experiments with prescribed atmospheric boundary conditions. We give two values here, 'at peak' and at the end of the ramp-down period. With elevated atmospheric pCO_2 (and climate warming) there are also land feedbacks, not considered further in our analysis. These land feedbacks case a net CO_2-uptake for the scenarios considered here, which increases the total cumulative compatible emissions with respect to the Earth System. Peak ΔDIC is the maximum marine ΔDIC observed. Year of peak is relative to yr 0. Intersection point is the year when $\Delta DICremin = \Delta DICpre$. Peak ΔDIC^{remin} is the maximum excess DIC^{remin} in the ocean. For $4xCO_2$ experiments peak pCO_2^{atm} is in yr 140, while it is in yr 70 for all $2xCO_2$ experiments. For details on the experiments, see the Online and SI Methods sections.

Experiment	Cumulative emissions at pCO_2-peak (at the end of ramp-down) [Pg C]	Peak ΔDIC [Pg C] (year of peak, [years])	Intersection point [years]	Peak ΔDIC^{remin} [Pg C] (year of peak, [years])
(2xCO2_) REVERSE	853 (177)	281 (88)	297	41(129)
2xCO2_slowcirc	841 (167)	268 (87)	343	38(129)
2xCO2_fastcirc	861 (184)	291 (88)	242	43 (132)
2xCO2_slowsink	850 (174)	278 (88)	273	39 (126)
2xCO2_fastsink	856 (182)	285 (88)	494	41 (134)
2xCO2_0.9	853 (178)	284 (91)	300	42 (135)
2xCO2_0.8	853 (180)	289 (94)	306	44 (144)
2xCO2_0.7	853 (185)	295 (99)	323	47 (152)
2xCO2_0.6	853 (188)	303 (106)	333	50 (167)
2xCO2_0.5	853 (194)	314 (116)	337	54 (184)
2xCO2_0.4	853 (203)	329 (131)	363	60 (219)
2xCO2_0.3	853 (217)	354 (158)	406	69 (263)
2xCO2_0.2	853 (236)	398 (210)	never[§]	85 (329)
2xCO2_0.1	855 (249)	never[§]	never[§]	never[§]
4xCO2(_REVERSE)	2396 (378)	790 (172)	415	100 (230)

[§] never, until year 500

Tab. S3: Metrics of time integrated CO_2-uptake of our default model variant ran with historical CO_2-emission forcing [6] and compared against a respective no-emission drift experiment.

Time period	This model ([6])	Reference value	Reference publication
	Pg C		
1994-2007, global	28.2	33.7 ± 4.0	[16]
1994-2007, Pacific Ocean	13.2	13.2 ± 1.3	[16]
1994-2007, Atlantic Ocean	7.5	11.9 ± 1.3	[16]
1994-2007, Indian Ocean	7.5	7.1 ± 3.4	[16]
1870-1995 (global)	96.6	97 ± 8	[17]
1780-2005, global	128.2	142.8	[18]

Reference values from [16] is based on observations. Reference value from [17] is CMIP5 model mean ($\pm$ std) based on 20 year mean values around 1870 and 1995, respectively. For the estimate from [18] we summed up their historical budget until the end of the historical period of the CMIP5 forcing used in [6].
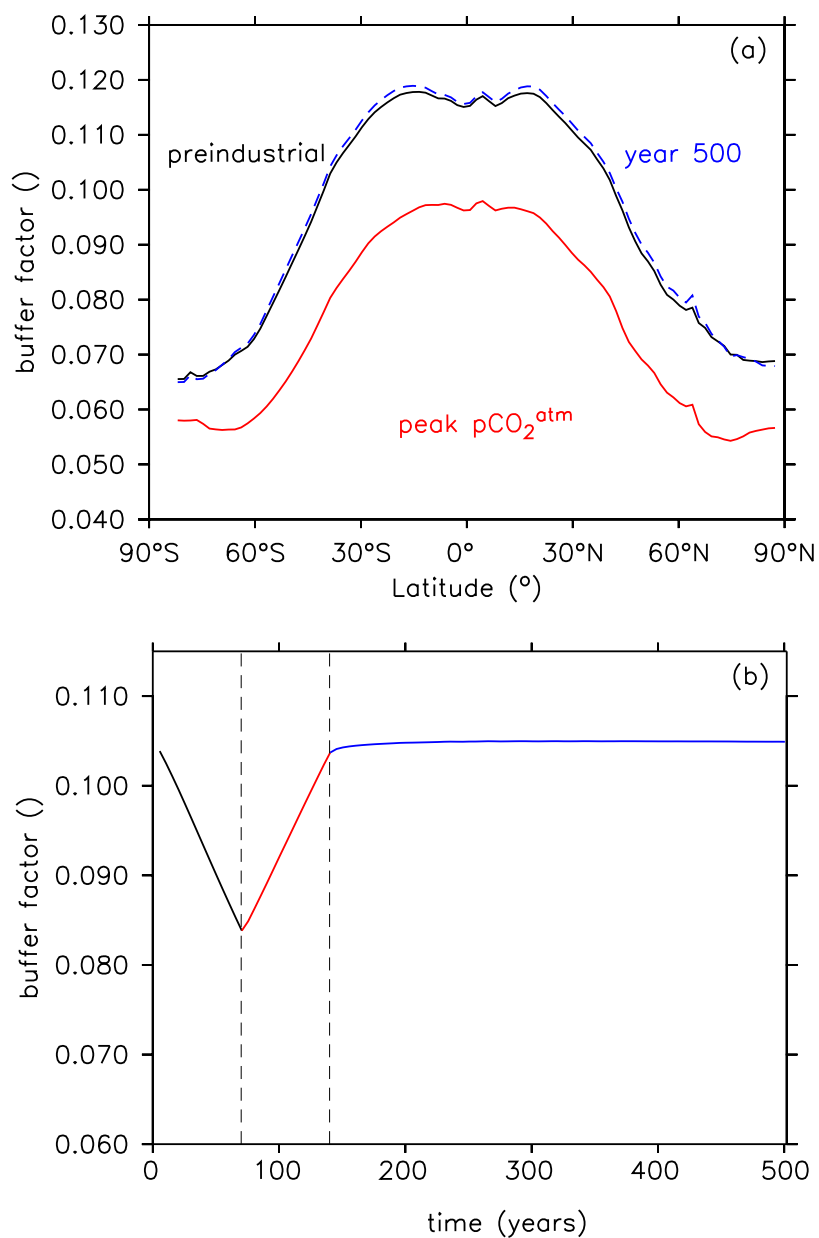
Fig. S1. CO_2-buffer factor, the fractional change of DIC per fractional change of pCO_2 ($\delta DIC/\delta pCO_2$), computed as the inverse of the Revelle-factor. (a) Zonal averages of surface ocean CO_2-buffer factor for preindustrial (black), at peak pCO_2^{atm} (year 70, red) and in year 500 (blue, dashed). (b) globally averaged CO_2-buffer factor over time (color coding as in Fig. 1).
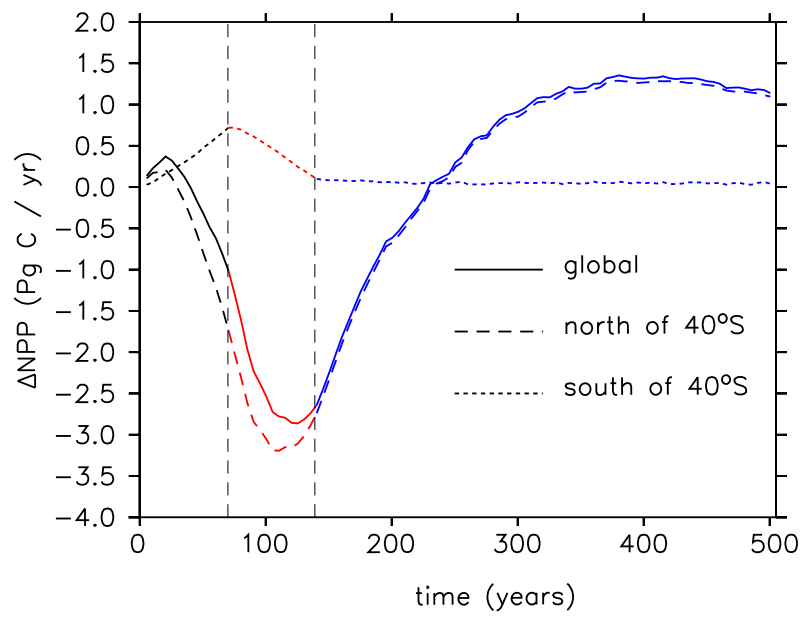
Fig. S2. Change in net primary production (NPP, Pg C / yr) integrated globally (solid lines), north of 40°S (long-dashed lines) and south of 40°S (short-dashed lines. Vertical lines indicate the end of ramp-up and of ramp-down periods, respectively (color coding as in Fig. 1).
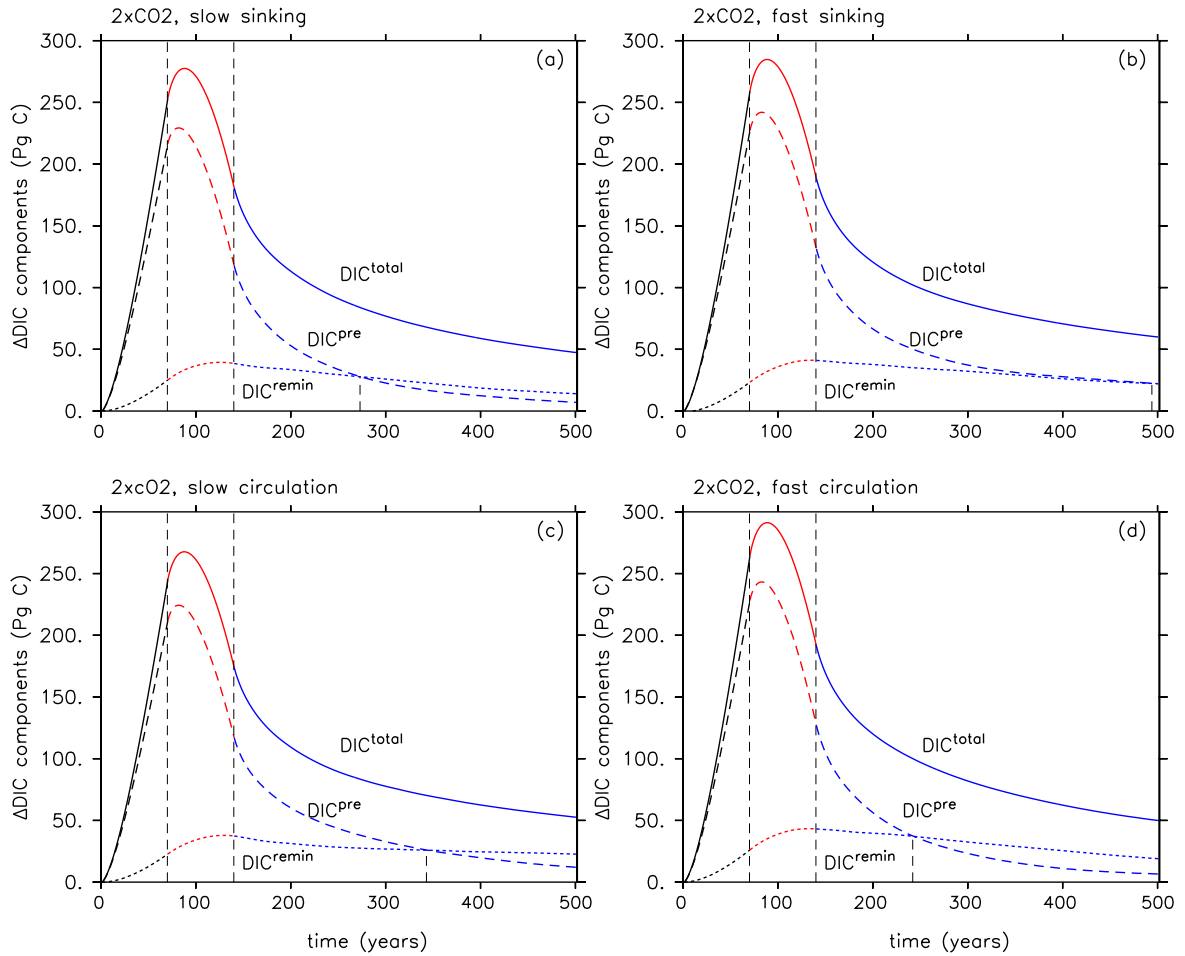
Fig. S3. Excess DIC (ΔDIC, Pg C) components from sensitivity experiments with modified ocean physics or biogeochemistry. ΔDIC-components using (a) a model variant with lower sinking speed increase with depth, (b) a model variant with higher sinking speed increase with depth, compared to the default model variant. Both variants (a, b) used the same parameterization of the model physics. ΔDIC-components using (c) a model variant with slightly lower maximum overturning, (d) a variant with slightly higher maximum overturning, compared with the default model. Sinking speed for both model variants (c, d) was like in the default model. Note that all model variants had been spun up with the respective parameterizations under preindustrial pCO_2 and climate forcing. See Online Methods and Tab. S2 for details. Vertical lines indicate times of peak pCO_2 (year 70), when pCO_2^{atm} is at the preindustrial level again (year 140), and the intersection point ($\Delta DIC^{remin} = \Delta DIC^{pre}$). Color code is like in Fig. 1.
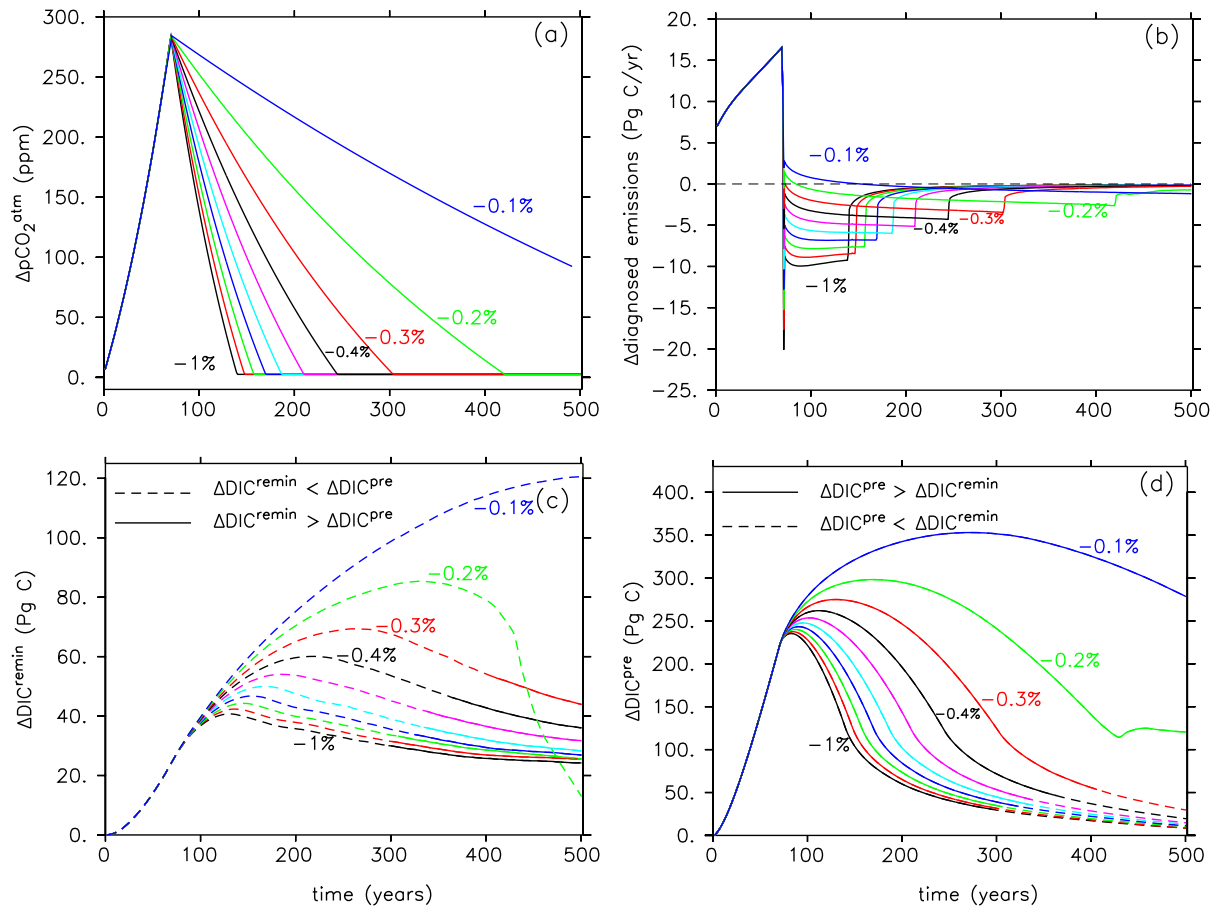
Fig. S4. Sensitivity experiments with differing atmospheric pCO_2 reduction rates during ramp-down ranging from -1%/year (REVERSE) to -0.1%/year () in -0.1%/year steps (see legend). Anomalies to preindustrial are shown. (a) prescribed pCO_2^{atm} path; (b) diagnosed compatible CO_2-emissions; (c) ΔDIC^{remin}, with solid lines indicating experiments and time periods where $\Delta DIC^{remin} > \Delta DIC^{pre}$; (d) ΔDIC^{pre} with solid lines indicating $\Delta DIC^{pre} > \Delta DIC^{remin}$.
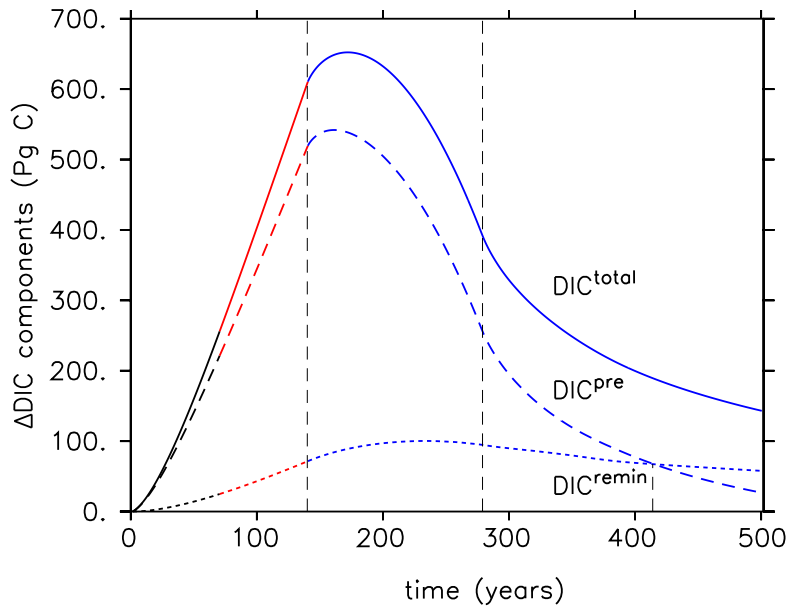
Fig. S5. Sensitivity experiment with 1%pCO_2^{atm} increase until reaching 4xpCO_2 and follow up -1%pCO_2^{atm} decrease until returning to preindustrial pCO_2. Globally integrated excess total dissolved inorganic carbon (ΔDIC, Pg C, solid lines), preformed DIC (DIC^{pre}, Pg C , long-dashed lines) and DIC attributable to the biological carbon pump (DIC^{remin}, Pg C, short-dashed lines). Black lines indicate the ramp-up period (pCO_2^{atm} increases), red lines the ramp-down period (pCO_2^{atm} decreases), and blue lines the stabilization period with constant pCO_2^{atm} simulated until year 500. Vertical lines indicate the end of ramp-up (peak pCO_2^{atm}, year 140) and of the ramp-down period (year 280), respectively. A third vertical dashed line indicates the intersection point ($\Delta DIC^{remin} = \Delta DIC^{pre}$).
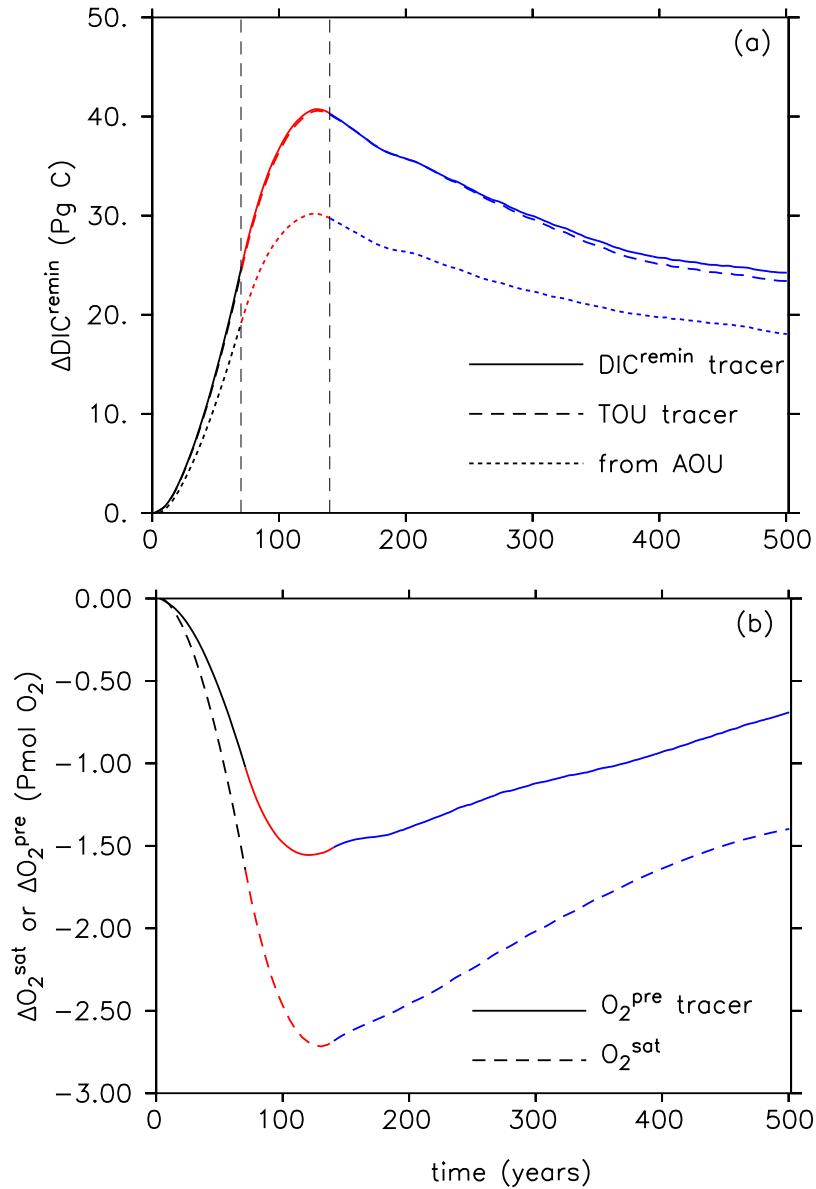
Fig. S6. Comparison of different ΔDIC^{remin} estimates for experiment REVERSE. (a) ΔDIC^{remin} quantified from the DIC^{remin} tracer (solid), a true oxygen utilization tracer (TOU-tracer), and from AOU (short dashed line). The AOU based estimate of ΔDIC^{remin} is lower by about 23.1 (±2.7)% compared to the estimate from the DIC^{remin} tracer. (b) Comparison of the change in preformed oxygen, ΔO_2^{pre}, quantified by an explicit preformed O_2 model tracer (defined similar to DIC^{pre}) and the change in oxygen saturation ΔO_2^{sat}, with oxygen saturation computed offline from potential temperature and salinity. $\Delta O_2^{pre} - \Delta O_2^{sat}$ measures the oxygen disequilibrium, which decreased during the experiment, which caused the AOU-based estimate of ΔDIC^{remin} (panel a) to be conservatively low.

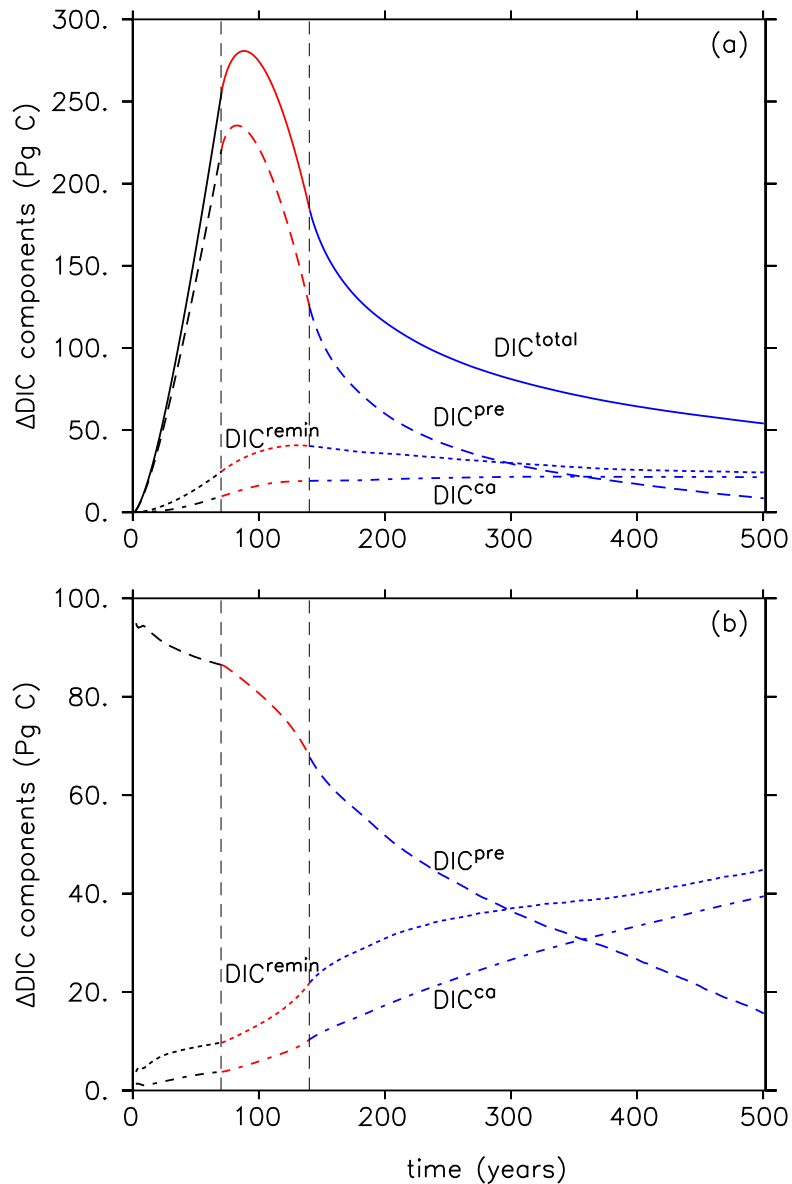Fig. S7. Absolute (a) and relative (b) changes of DIC components from experiment REVERSE. (a) In addition to ΔDIC (solid lines), ΔDIC^{pre} (long-dashed lines), and ΔDIC^{remin} (short-dashed lines), we show ΔDIC^{ca}, the change of DIC attributable to the $CaCO_3$ pump. ΔDIC^{ca} was computed as residual of $\Delta DIC - \Delta DIC^{pre} - \Delta DIC^{remin}$. Note that unlike ΔDIC^{pre} and ΔDIC^{remin}, ΔDIC^{ca} constitutes only an apparent marine carbon sink since it is accompanied by a twice as large change in total alkalinity in the interior ocean. An increase (decrease) of ΔDIC^{ca} goes along with a decrease (increase) in surface alkalinity since total alkalinity is conserved in the ocean on times scales of the experiments, except for minor changes related to the alkalinity effect of denitrification and N_2-fixation (not shown). A decreasing surface alkalinity over the course of the experiment contributes to the carbon-climate feedback processes reducing DIC^{pre}. (b) Relative changes of DIC components in percent of total DIC. Color code and vertical lines like in Fig. 1.
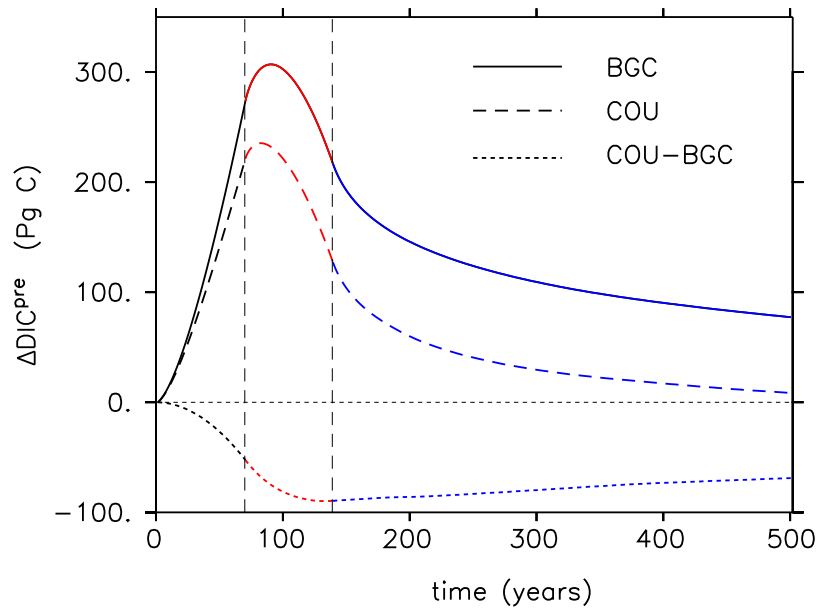
Fig. S8. ΔDIC^{pre} from experiment REVERSE run in fully coupled (COU, long-dashed lines) and biogeochemically-only coupled mode (BGC, solid line). ΔDIC^{pre} from the BGC experiment represents the uptake of anthropogenic CO_2 assuming no climate change. The difference of ΔDIC^{pre} from COU and BGC experiments (COU-BGC, short dashed line), represents the combined effect of various carbon-climate feedbacks on ΔDIC^{pre}, for example from surface ocean warming on CO_2-solubility.

References (of SI)

1   Duteil, O. & Oschlies, A. Sensitivity of simulated extent and future evolution of marine suboxia to mixing intensity. *Geophys. Res. Lett.* **38**, L06607, doi: 06610.01029/02011GL046877 (2011).

2   Oschlies, A. A committed fourfold increase in ocean oxygen loss. *Nat Commun* **12** 2307 (2021). https://doi.org:10.1038/s41467-021-22584-4

3   Reith, F., Koeve, W., Keller, D. P., Getzlaff, J. & Oschlies, A. Meeting climate targets by direct CO2 injections: what price would the ocean have to pay? *Earth Syst Dynam* **10**, 711-727 (2019). https://doi.org:10.5194/esd-10-711-2019

4   Friedlingstein, P. *et al.* Climate-carbon cycle feedback analysis: Results from the (CMIP)-M-4 model intercomparison. *J Climate* **19**, 3337-3353 (2006). https://doi.org:Doi 10.1175/Jcli3800.1

5   Arora, V. K. *et al.* Carbon-concentration and carbon-climate feedbacks in CMIP6 models and their comparison to CMIP5 models. *Biogeosciences* **17**, 4173-4222 (2020). https://doi.org:10.5194/bg-17-4173-2020

6   Koeve, W., Kähler, P. & Oschlies, A. Does export production measure transient changes of the biological carbon pump's feedback to the atmosphere under global warming? *Geophys Res. Lett.* **47**, e2020GL089928 (2020). https://doi.org:10.1029/2020GL089928

7   Wilson, J. D. *et al.* The biological carbon pump in CMIP6 models: 21st century trends and uncertainties. *Proc. Natl. Acad. Sci. U. S. A.* **119**, e2204369119 (2022). https://doi.org:10.1073/pnas.2204369119

8   Koeve, W. & Kähler, P. Oxygen utilization rate (OUR) underestimates ocean respiration: A model study. *Global Biogeochemical Cycles* **30**, 1166-1182 (2016). https://doi.org:10.1002/2015gb005354

9   Keeling, R. F., Körtzinger, A. & Gruber, N. Ocean deoxygenation in a warming world. *Annu. Rev. Marine. Sci.* **2**, 199-229 (2010). https://doi.org/10.1146/annurev.marine.010908.163855

10   Schmidtko, S., Stramma, L. & Visbeck, M. Decline in global oceanic oxygen content during the past five decades. *Nature* **542**, 335-339 (2017). https://doi.org:10.1038/nature21399

11   Oschlies, A., Brandt, P., Stramma, L. & Schmidtko, S. Drivers and mechanisms of ocean deoxygenation. *Nature Geoscience* **11**, 467-473 (2018). https://doi.org:10.1038/s41561-018-0152-2

12   Oschlies, A. *et al.* Patterns of deoxygenation: sensitivity to natural and anthropogenic drivers. *Philos T R Soc A* **375** 20160325 (2017). https://doi.org:10.1098/rsta.2016.0325

13   Stramma, L., Oschlies, A. & Schmidtko, S. Mismatch between observed and modeled trends in dissolved upper-ocean oxygen over the last 50 yr. *Biogeosciences* **9**, 4045-4057 (2012). https://doi.org:10.5194/bg-9-4045-2012

14   Claustre, H., Johnson, K. S. & Takeshita, Y. Observing the Global Ocean with Biogeochemical-Argo. *Annual Review of Marine Science, Vol 12* **12**, 23-48 (2020). https://doi.org:10.1146/annurev-marine-010419-010956

15   Chen, H. D., Haumann, F. A., Talley, L. D., Johnson, K. S. & Sarmiento, J. L. The Deep Ocean's Carbon Exhaust. *Global Biogeochemical Cycles* **36** e2021GB007156 (2022). https://doi.org: 10.1029/2021GB007156

16   Gruber, N. *et al.* The oceanic sink for anthropogenic CO2 from 1994 to 2007. *Science* **363**, 1193-1199 (2019). https://doi.org:10.1126/science.aau5153

17   Frölicher, T. L. *et al.* Dominance of the Southern Ocean in Anthropogenic Carbon and Heat Uptake in CMIP5 Models. *J Climate* **28**, 862-886 (2015).

18   Friedlingstein, P. *et al.* Global Carbon Budget 2023. *Earth System Science Data* **15**, 5301-5369 (2023). https://doi.org:10.5194/essd-15-5301-2023